ADVANCED MATERIALS TECHNOLOGIES

Supporting Information

for *Adv. Mater. Technol.*, DOI 10.1002/admt.202300777

Impact of Side Chain Extension on the Morphology and Electrochemistry of Phosphonated Poly(Ethylenedioxythiophene) Derivatives

*Jonathan Hopkins, Daniel Ta, Antonio Lauto, Carly Baker, John Daniels, Pawel Wagner, Klaudia K. Wagner, Nigel Kirby, Claudio Cazorla, David L. Officer and Damia Mawad**

Supporting Information

Impact of side chain extension on the morphology and electrochemistry of phosphonated poly(ethylenedioxythiophene) derivatives

*Jonathan Hopkins, Daniel Ta, Antonio Lauto, John Daniels, Pawel Wagner, Klaudia K. Wagner, Nigel Kirby, Claudio Cazorla, David L. Officer, Damia Mawad**

Table of Contents

1 Synthesis and NMR spectroscopy

Scheme S1. Synthesis of PEDOT-Bu-Phos.

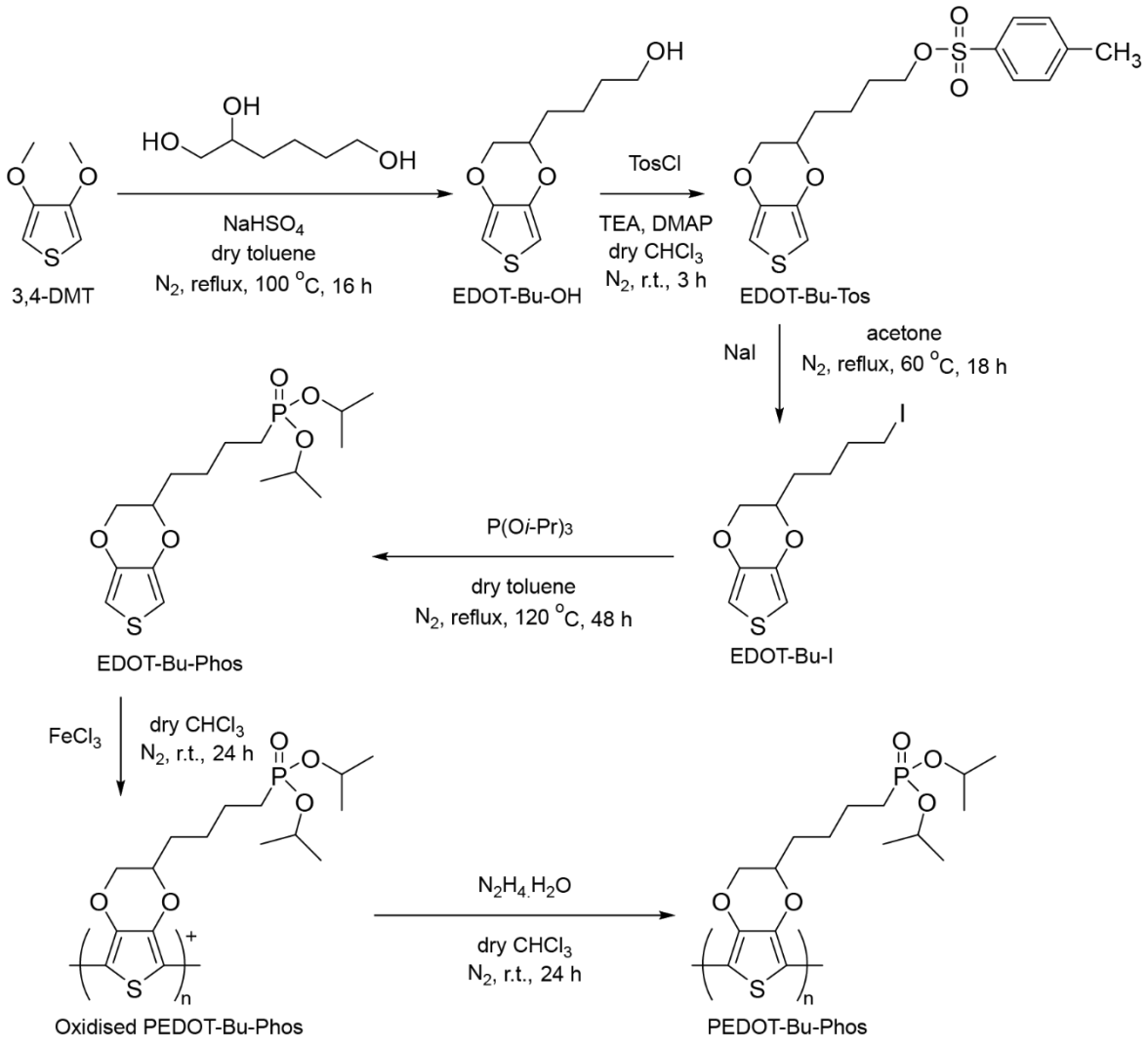

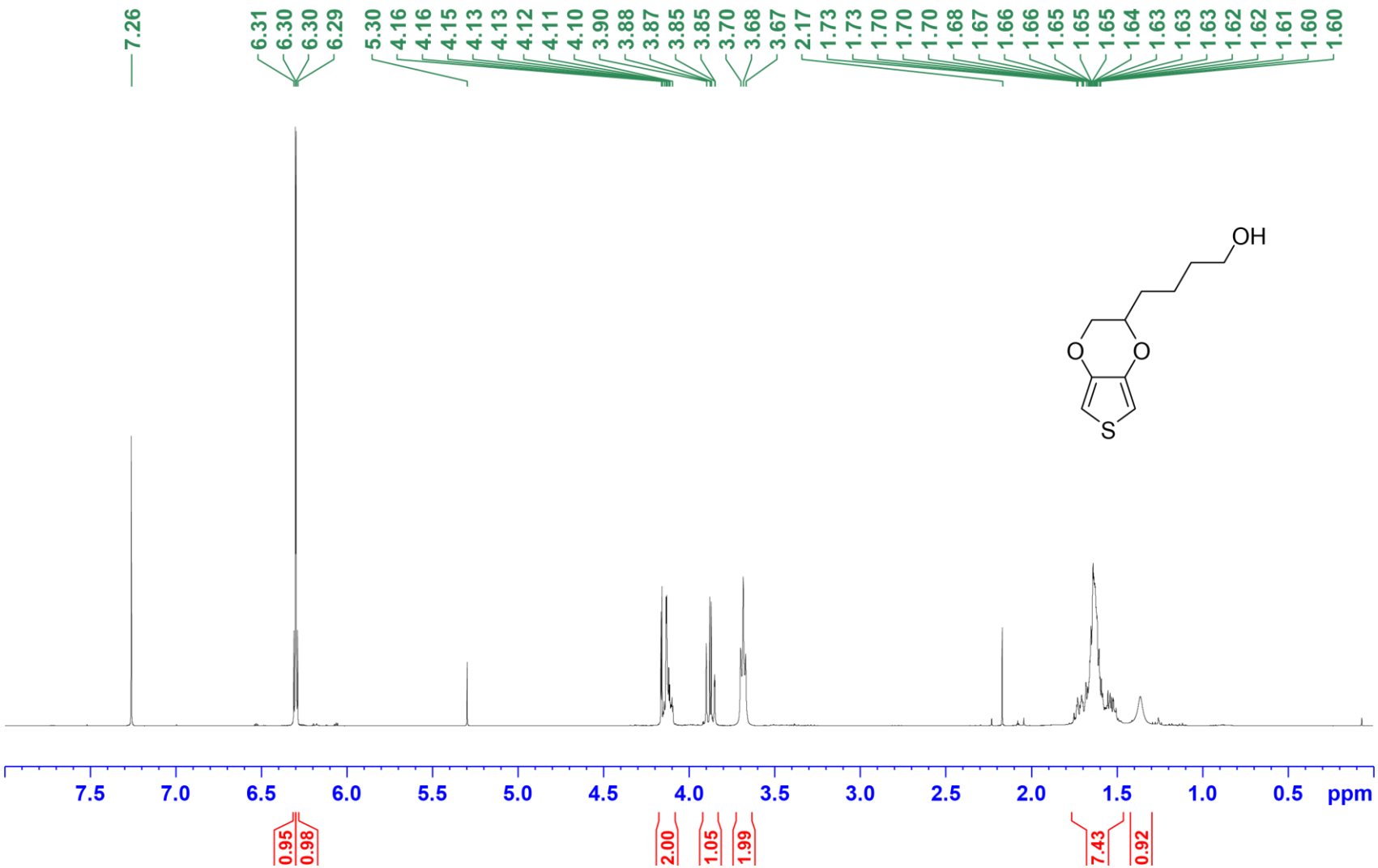

Figure S1. ^{1}H-NMR spectrum of EDOT-Bu-OH in $CDCl_3$.

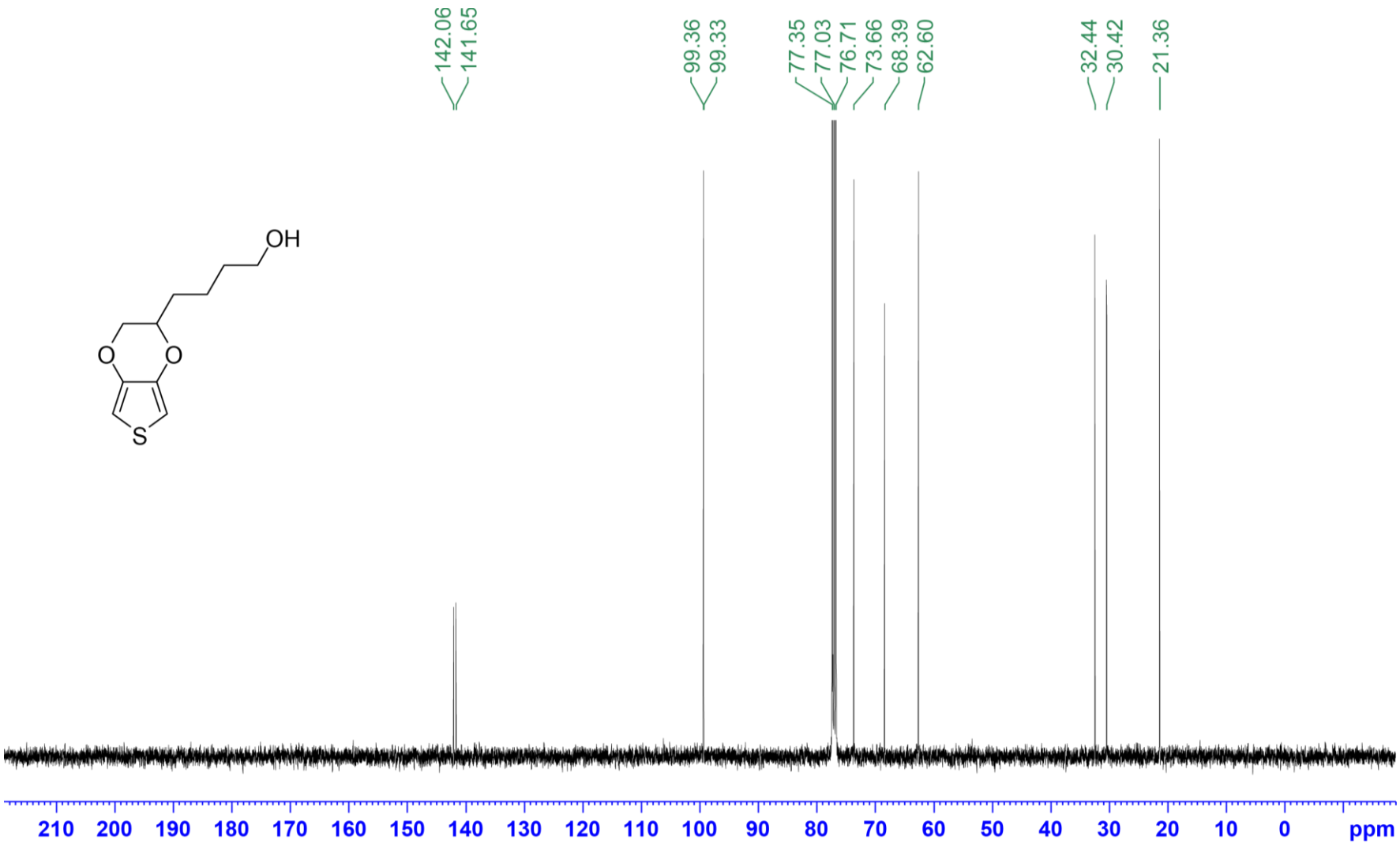

Figure S2. ^{13}C-NMR spectrum of EDOT-Bu-OH in $CDCl_3$.

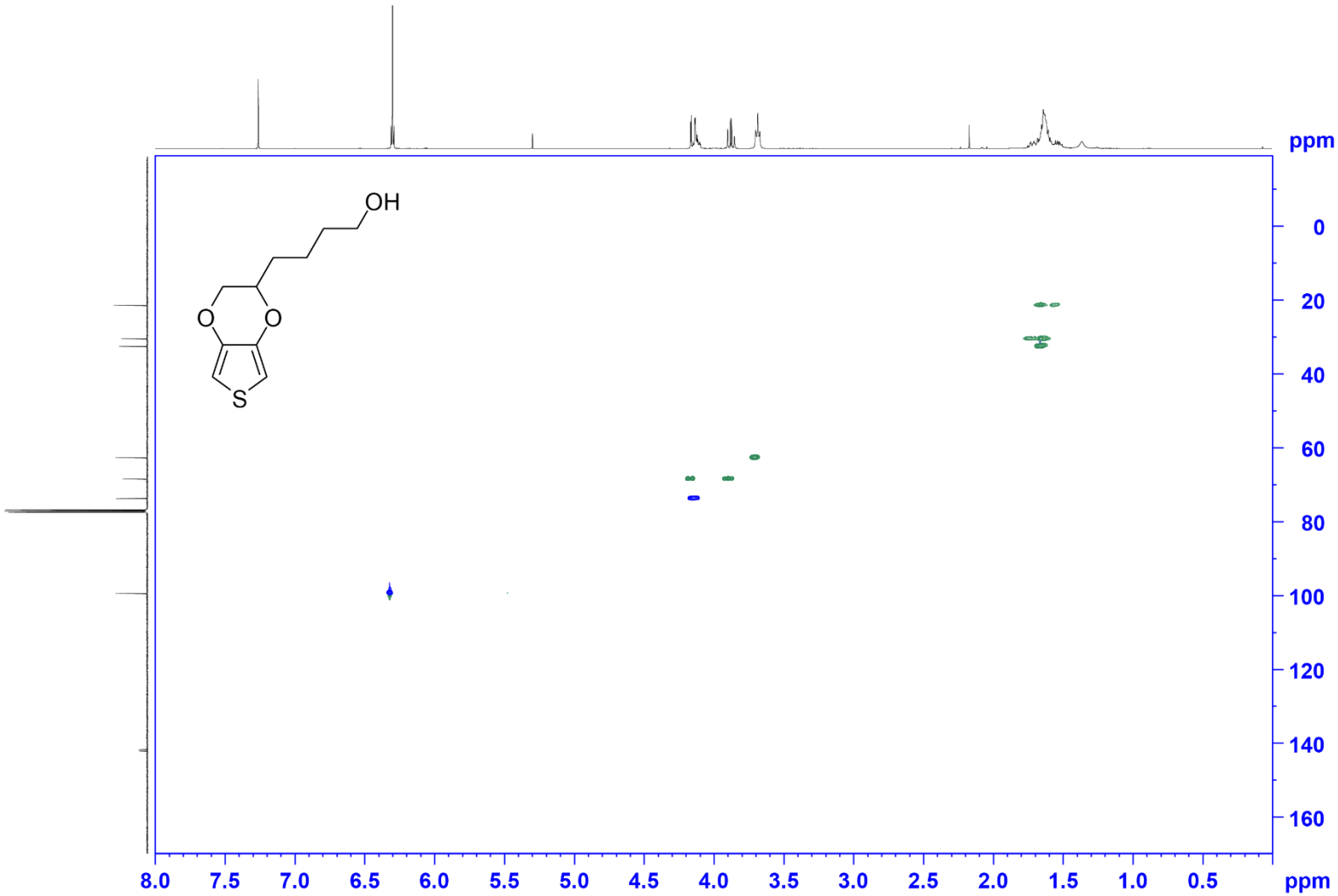

Figure S3. ^{1}H-^{13}C HSQC NMR spectrum of EDOT-Bu-OH in $CDCl_3$.

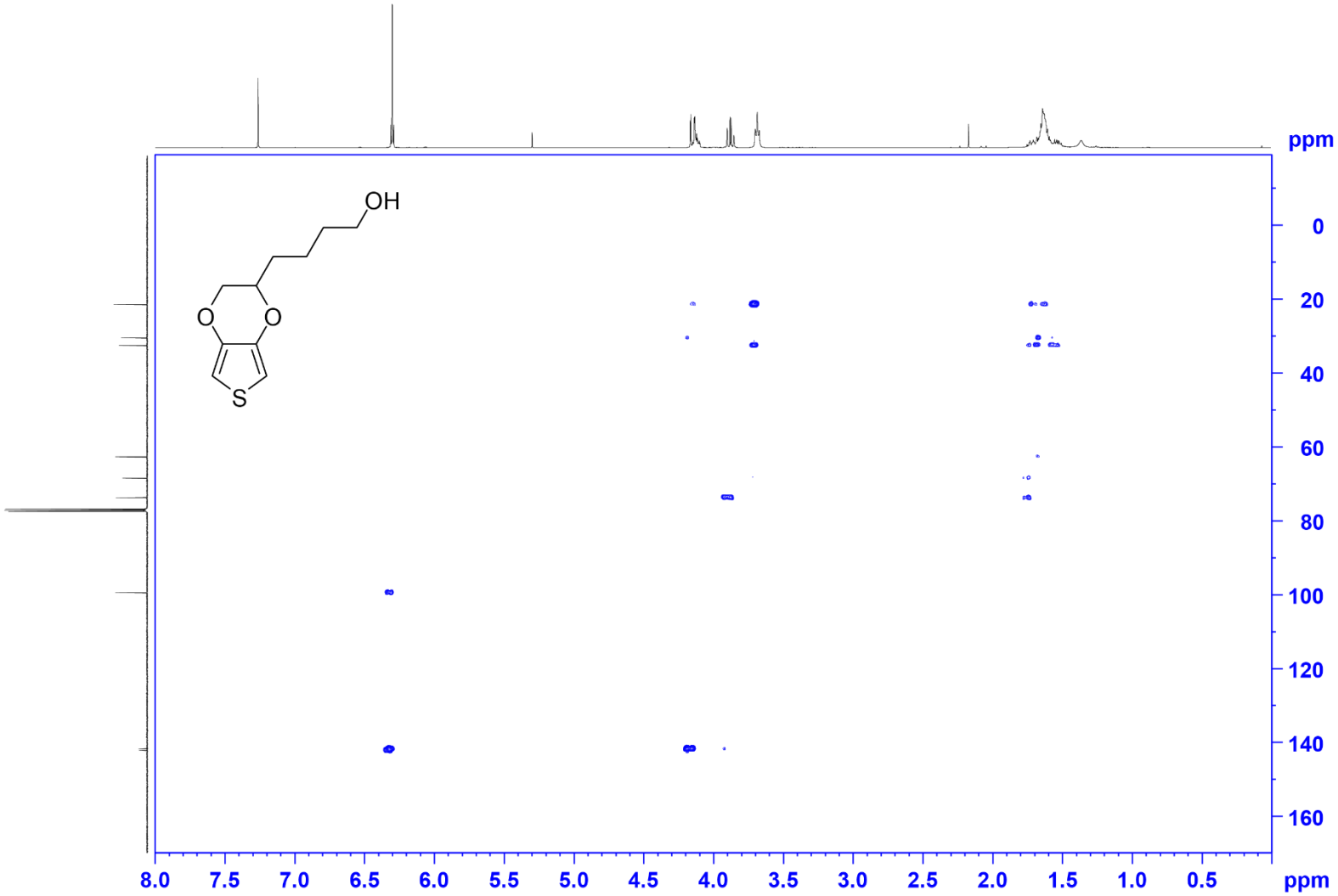

Figure S4. ^{1}H-^{13}C HMBC NMR spectrum of EDOT-Bu-OH in $CDCl_3$.

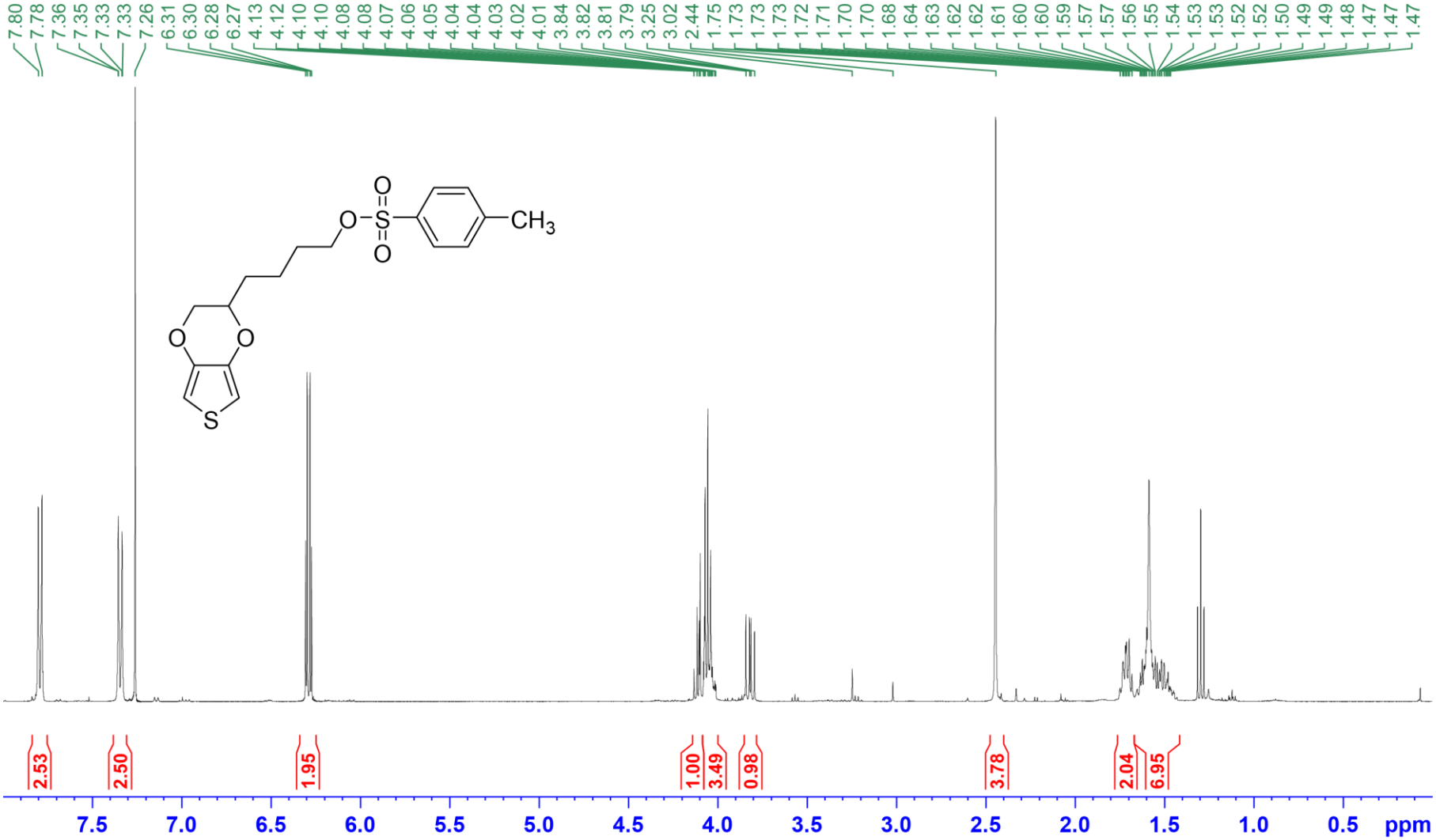

Figure S5. ^{1}H-NMR spectrum of EDOT-Bu-Tos in $CDCl_3$.

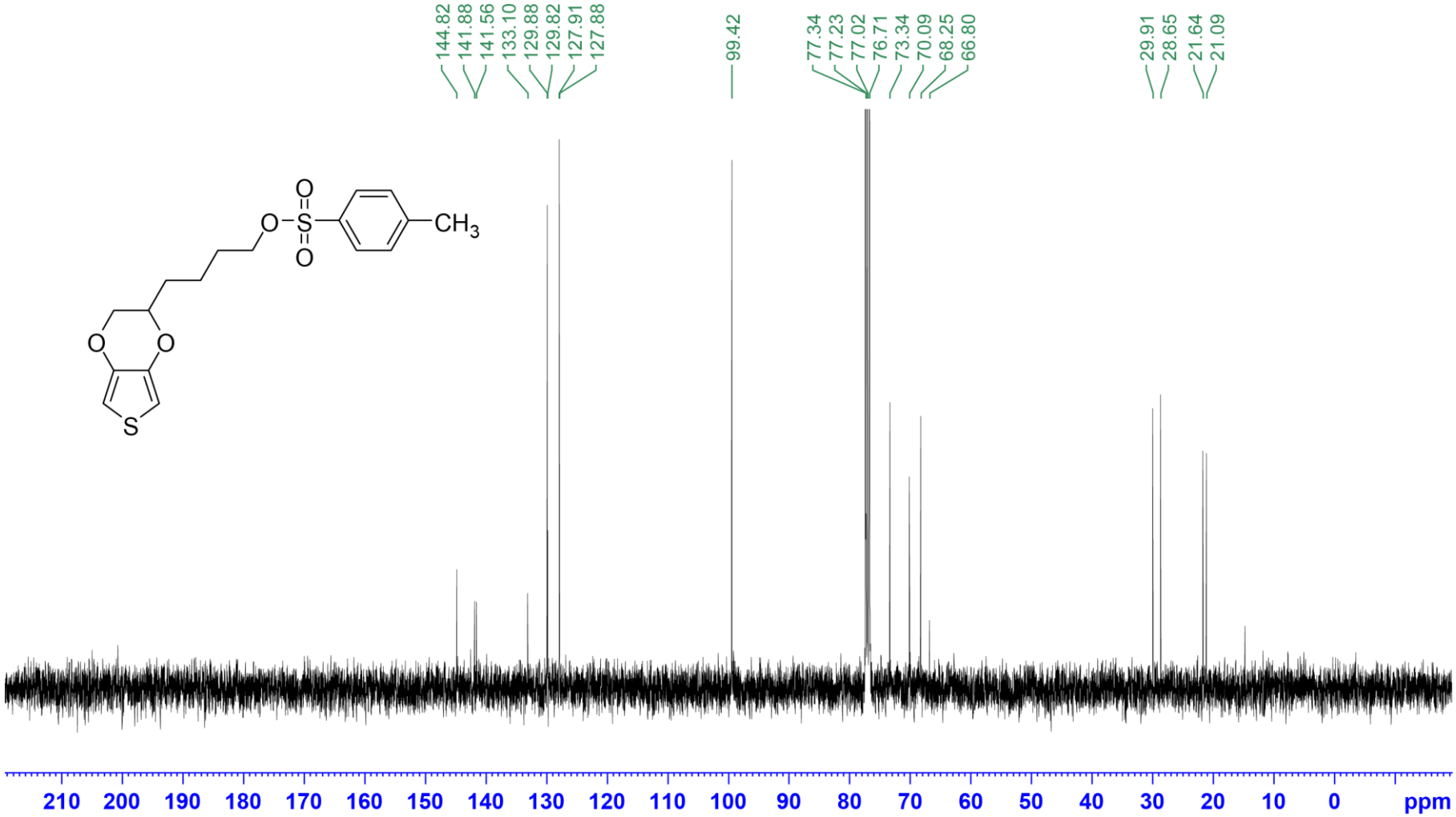

Figure S6. ^{13}C-NMR spectrum of EDOT-Bu-Tos in $CDCl_3$.

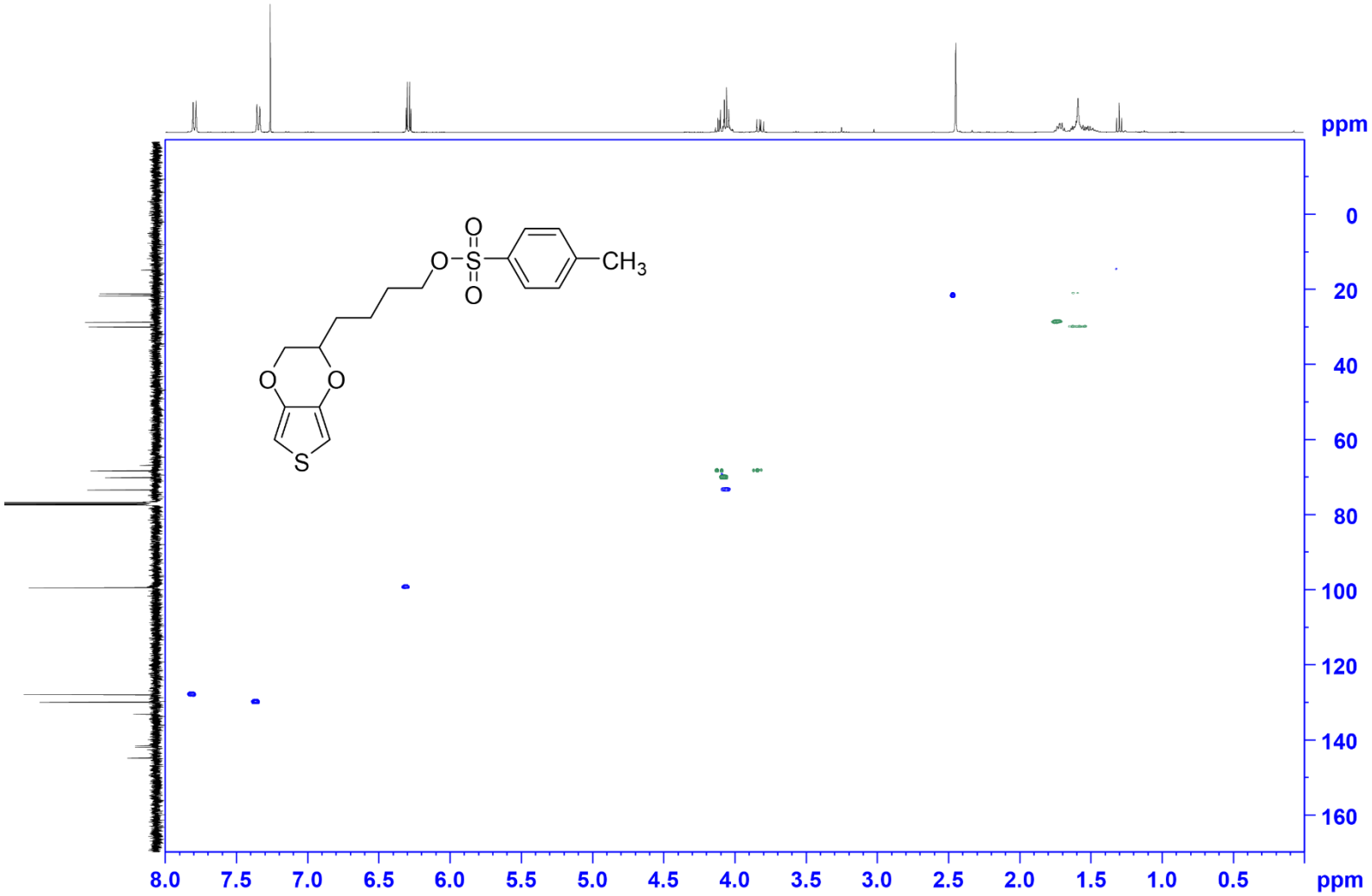

Figure S7. ^{1}H-^{1}3C HSQC NMR spectrum of EDOT-Bu-Tos in $CDCl_3$.

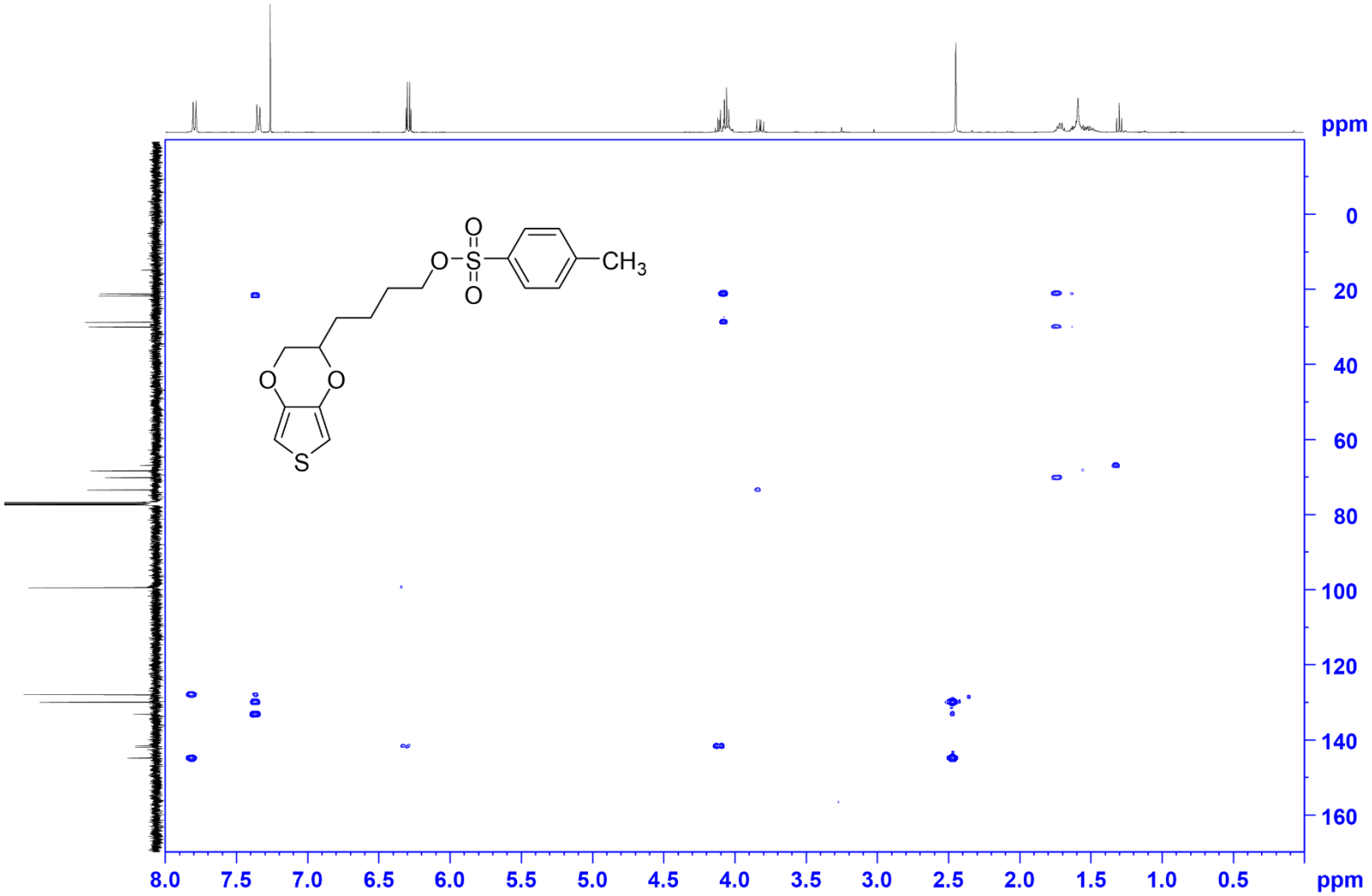

Figure S8. ^{1}H-^{1}3C HMBC NMR spectrum of EDOT-Bu-Tos in $CDCl_3$.

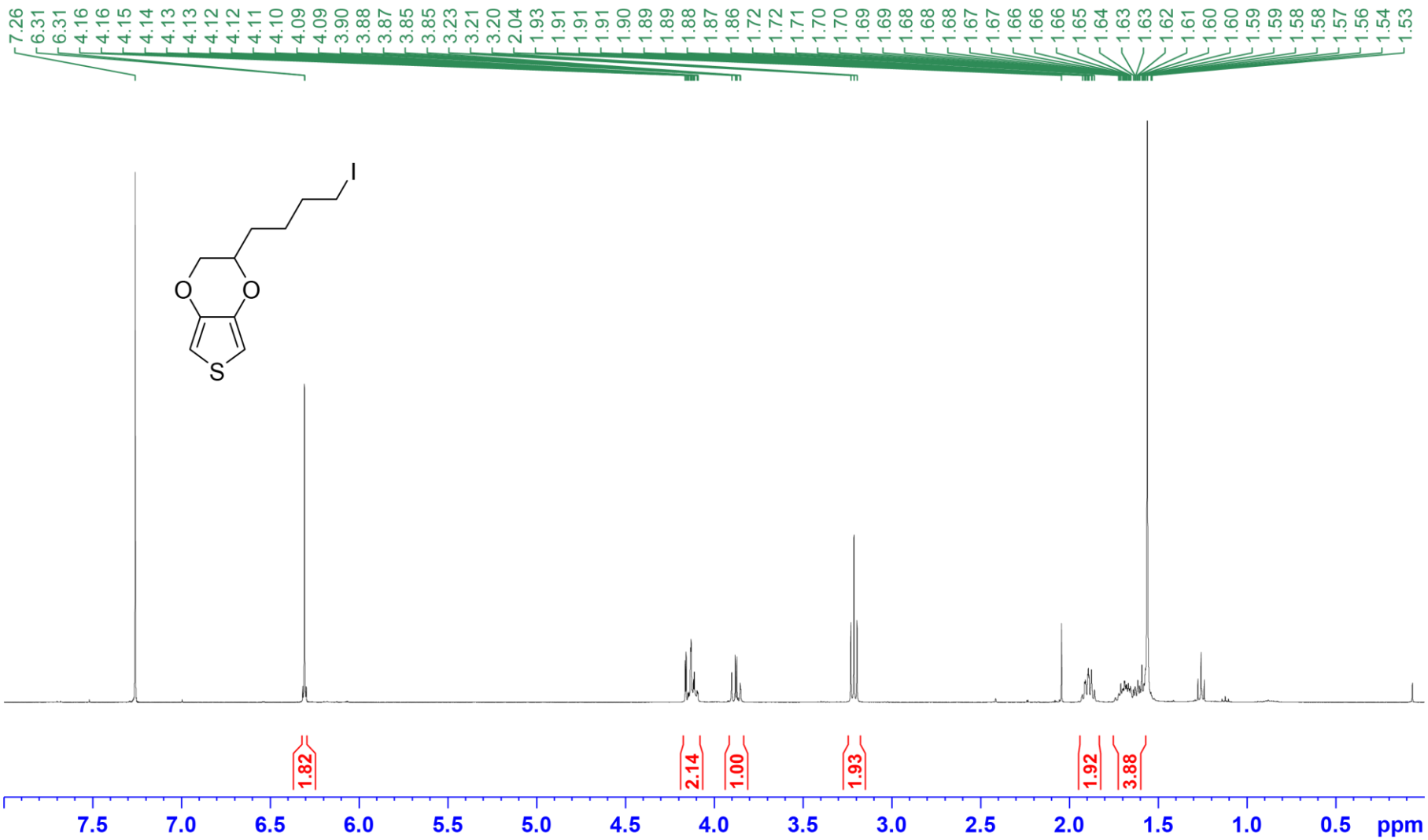

Figure S9. ^{1}H-NMR spectrum of EDOT-Bu-I in $CDCl_3$.

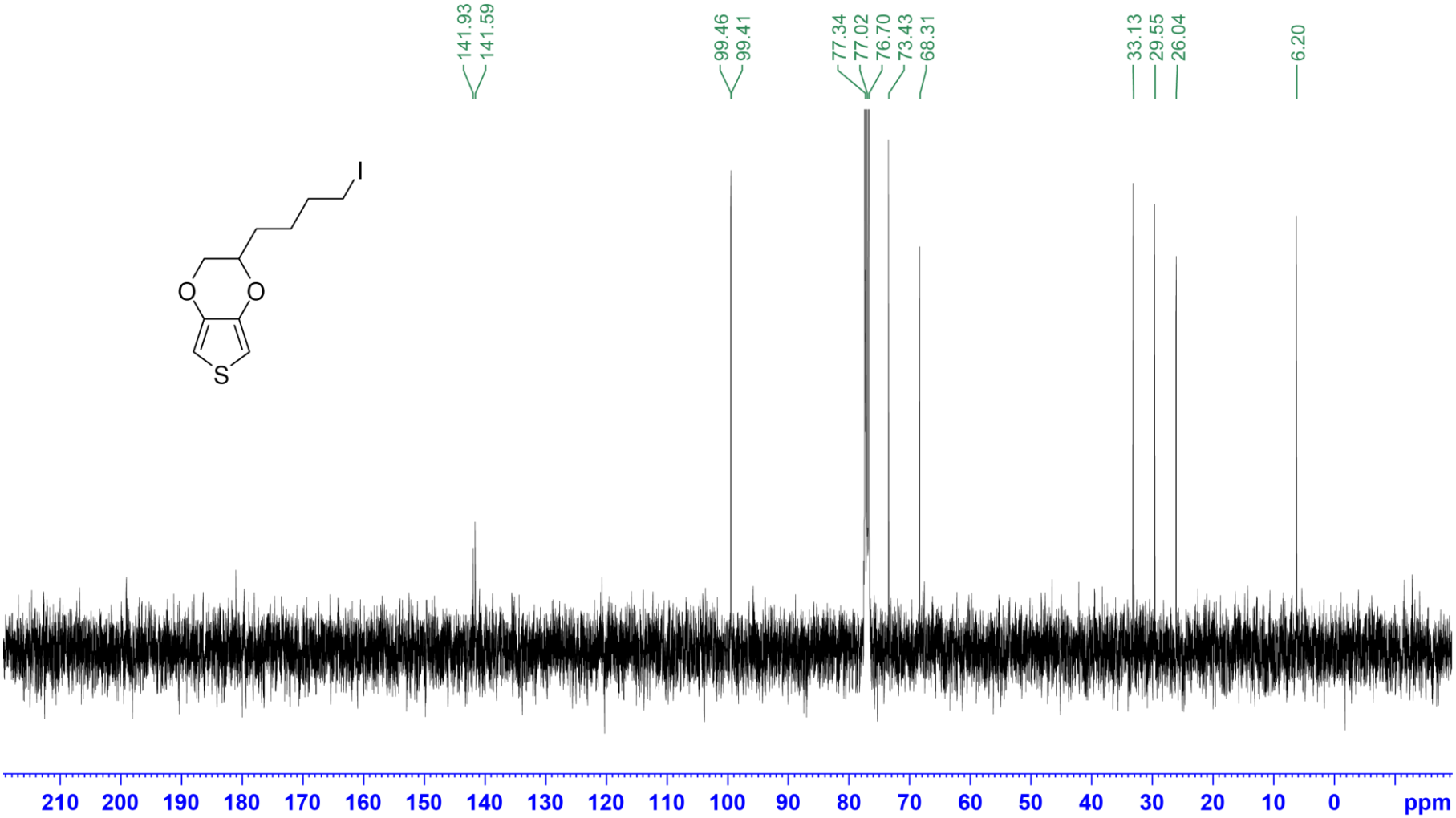

Figure S10. ^{13}C-NMR spectrum of EDOT-Bu-I in $CDCl_3$.

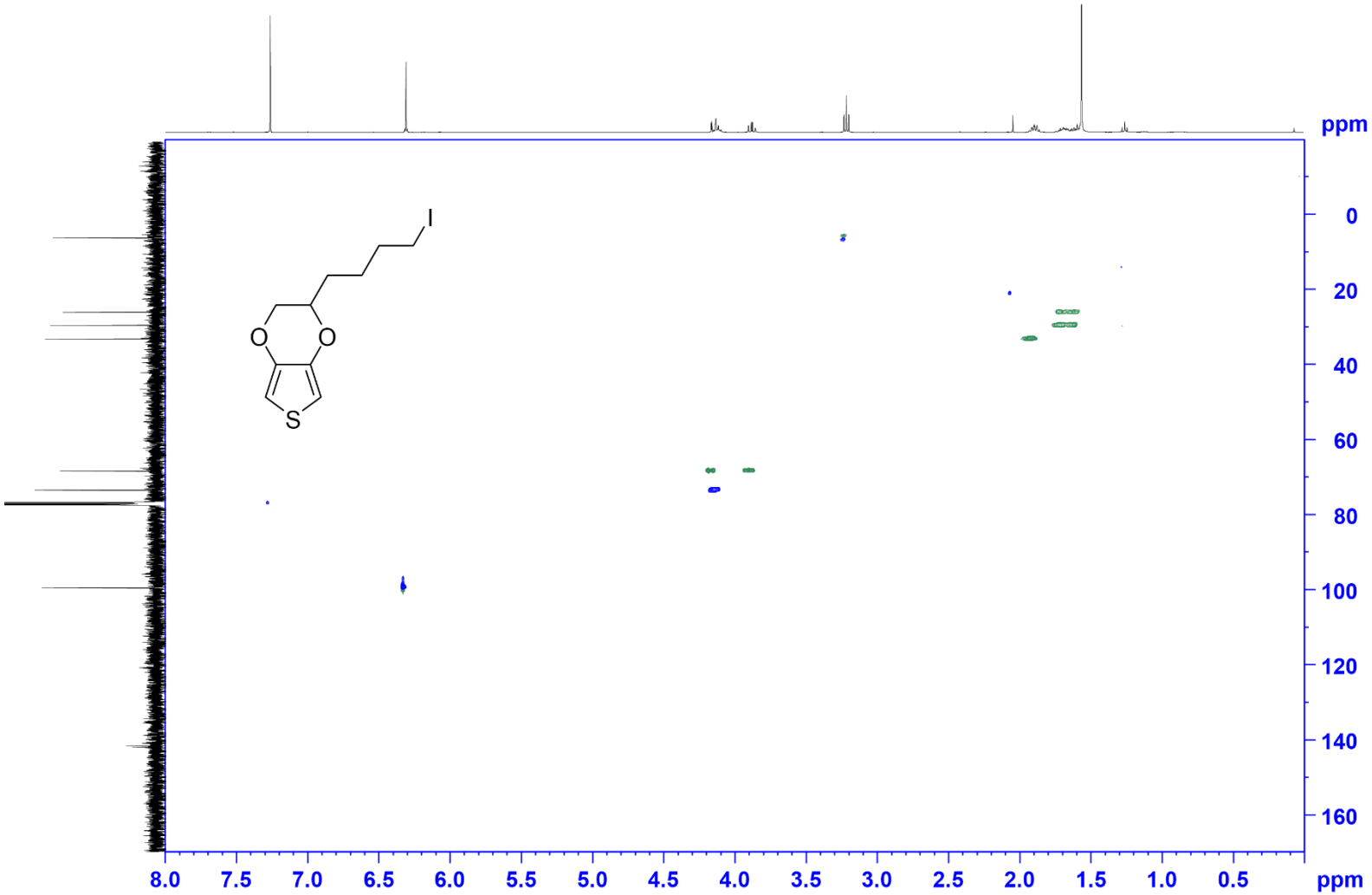

Figure S11. ^{1}H-^{1}3C HSQC NMR spectrum of EDOT-Bu-I in $CDCl_3$.

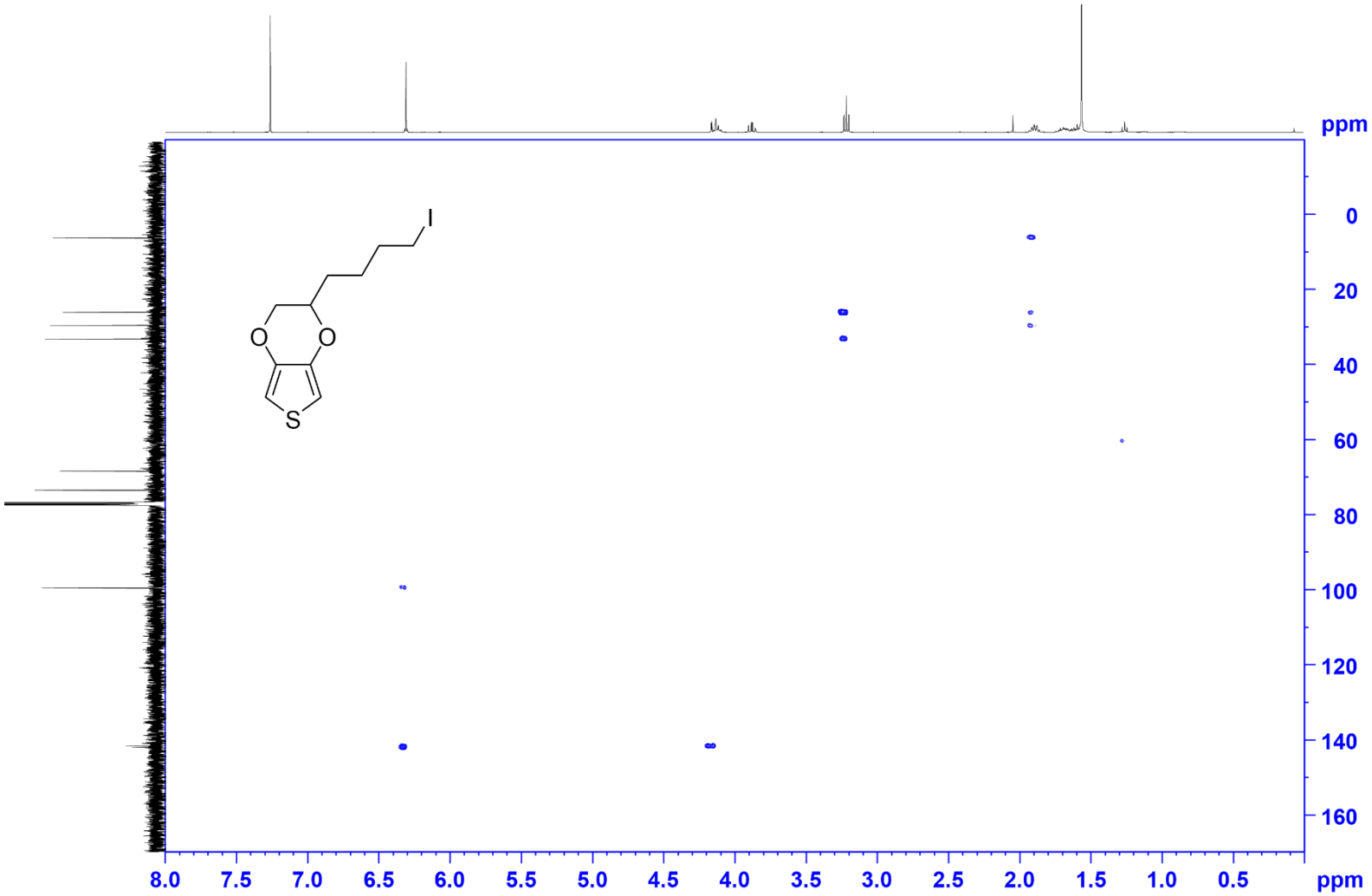

Figure S12. ^{1}H-^{1}3C HMBC NMR spectrum of EDOT-Bu-I in $CDCl_3$.

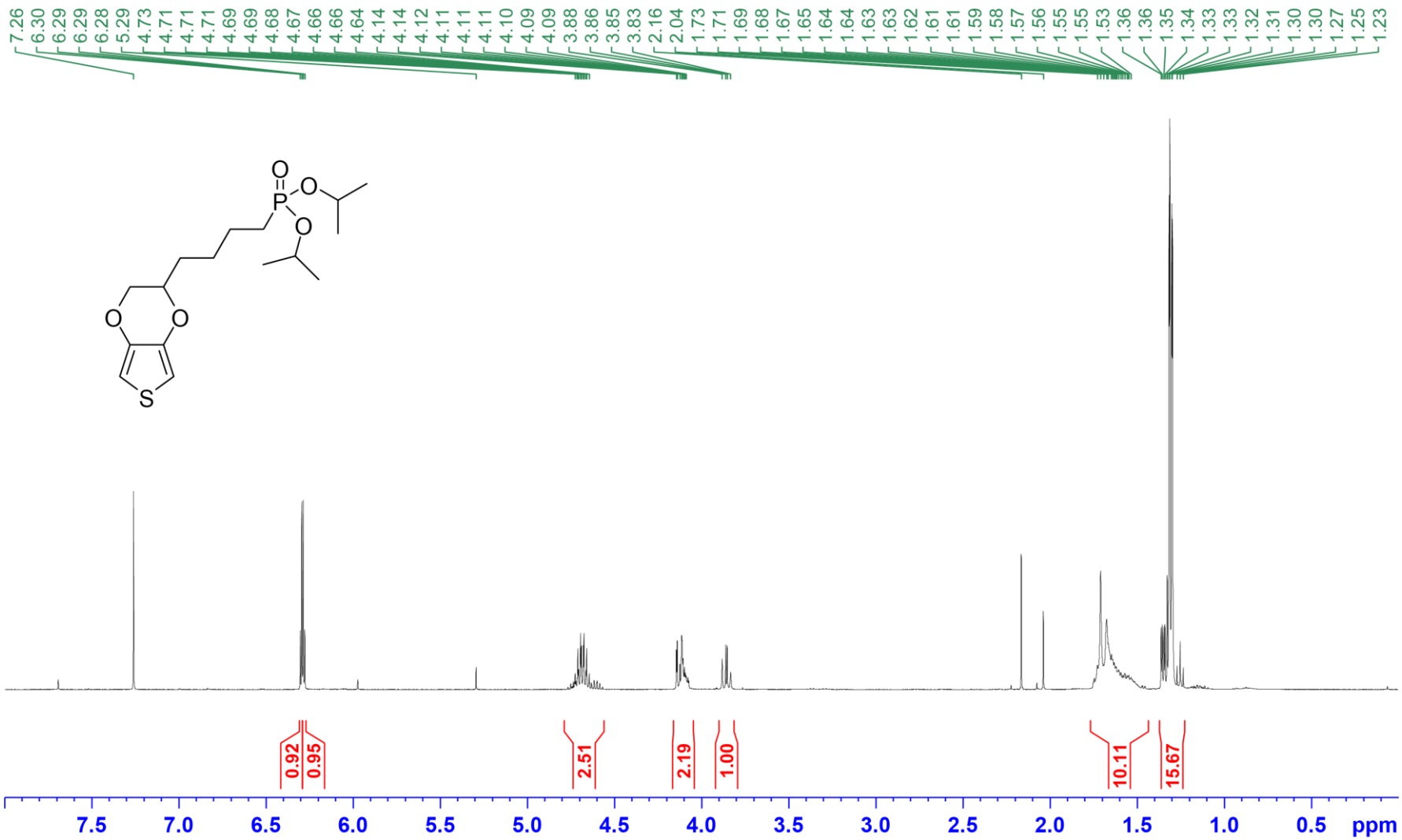

Figure S13. ^{1}H-NMR spectrum of EDOT-Bu-Phos in $CDCl_3$.

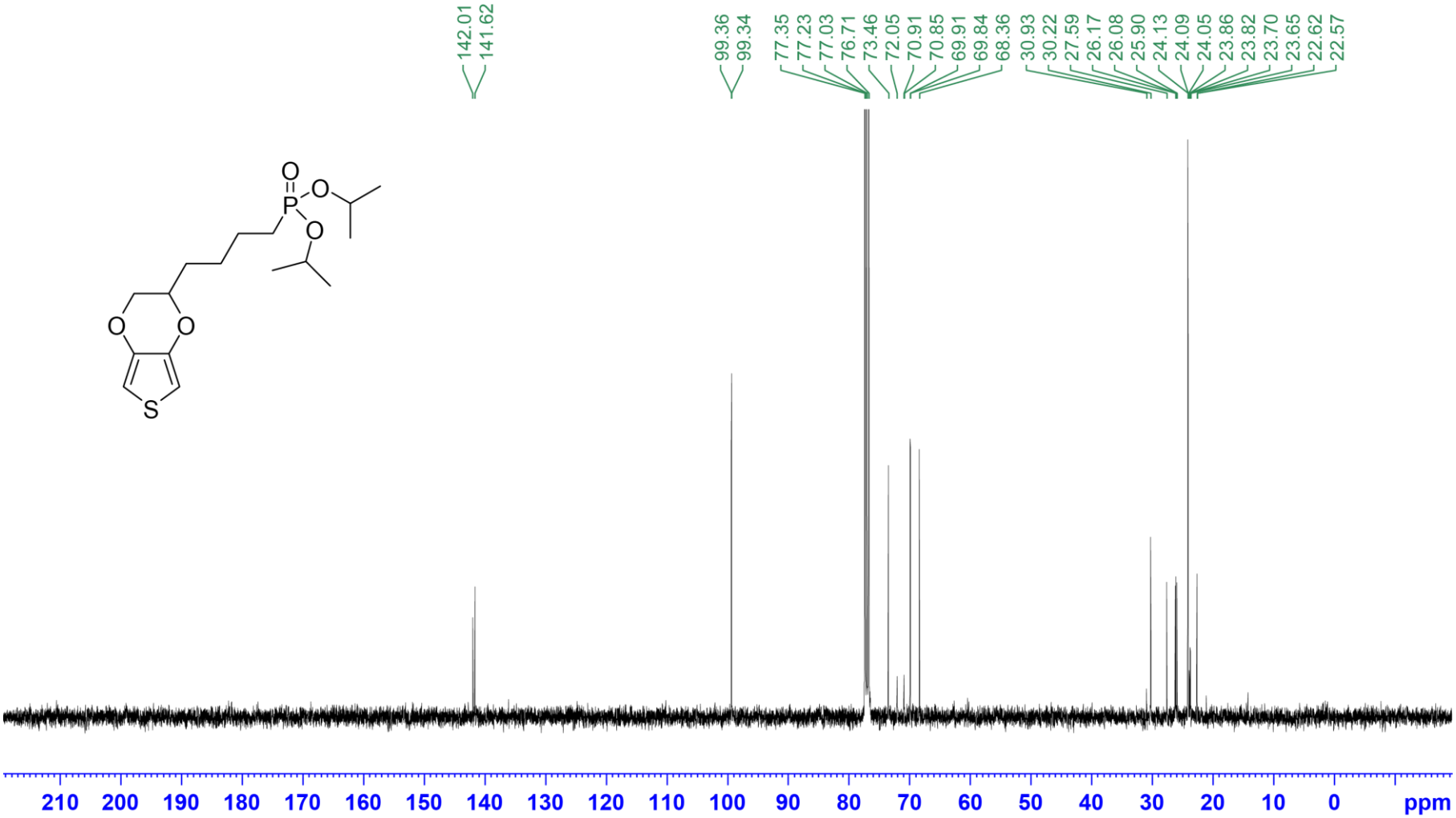

Figure S14. ^{13}C-NMR spectrum of EDOT-Bu-Phos in $CDCl_3$.

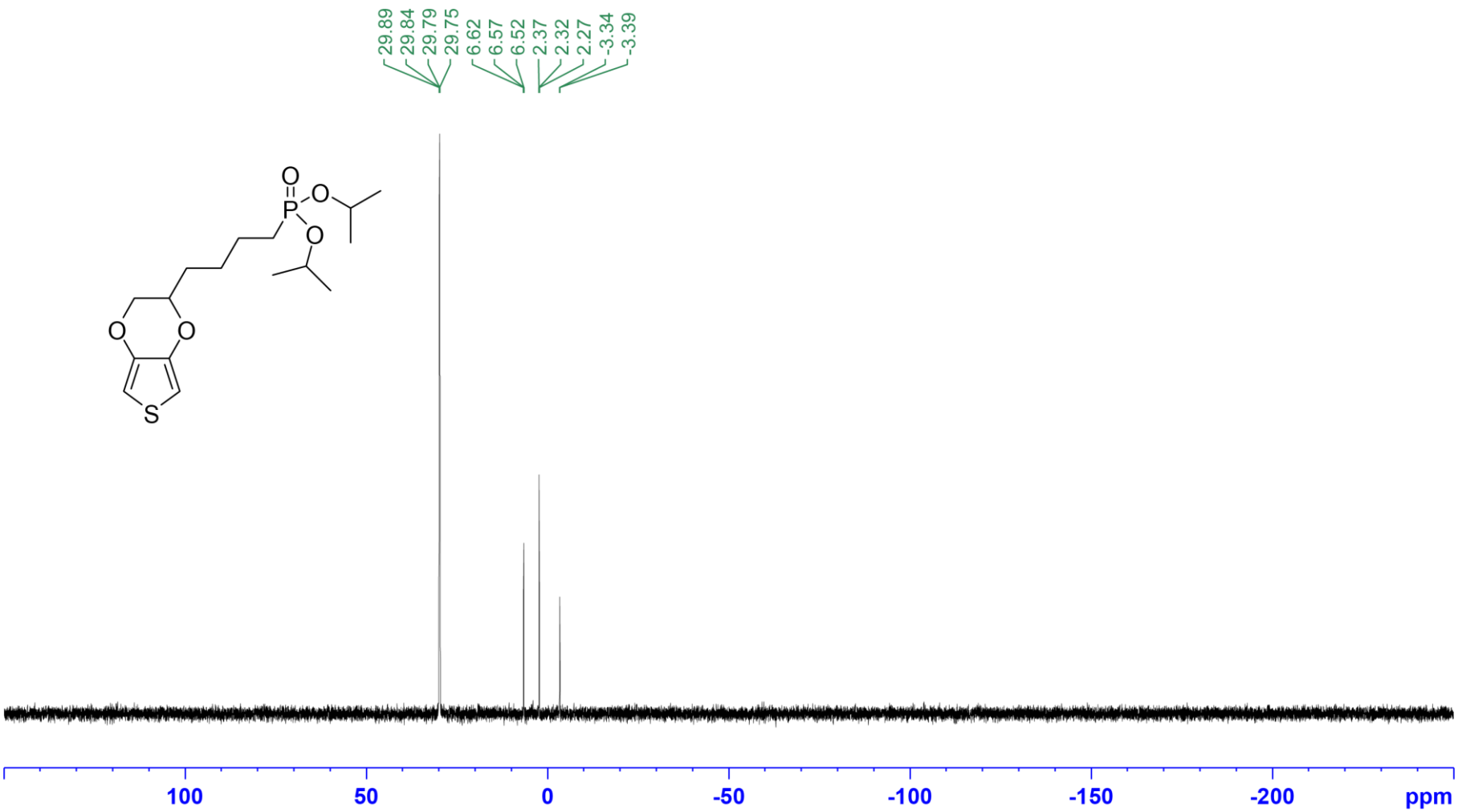

Figure S15. ^{31}P-NMR spectrum of EDOT-Bu-Phos in $CDCl_3$.

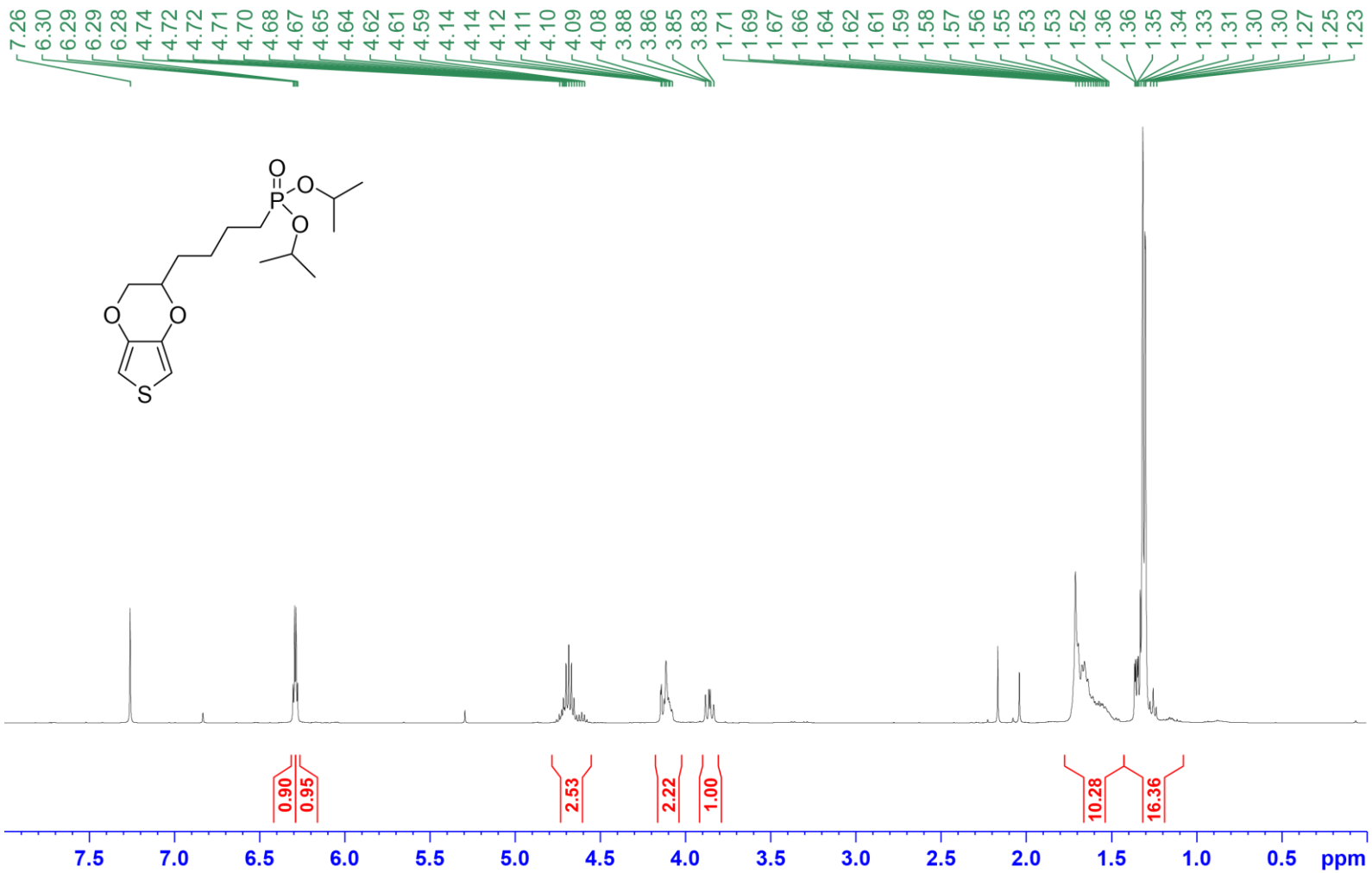

Figure S16. $^{1}H\{^{31}P\}$-decoupled NMR spectrum of EDOT-Bu-Phos in $CDCl_3$.

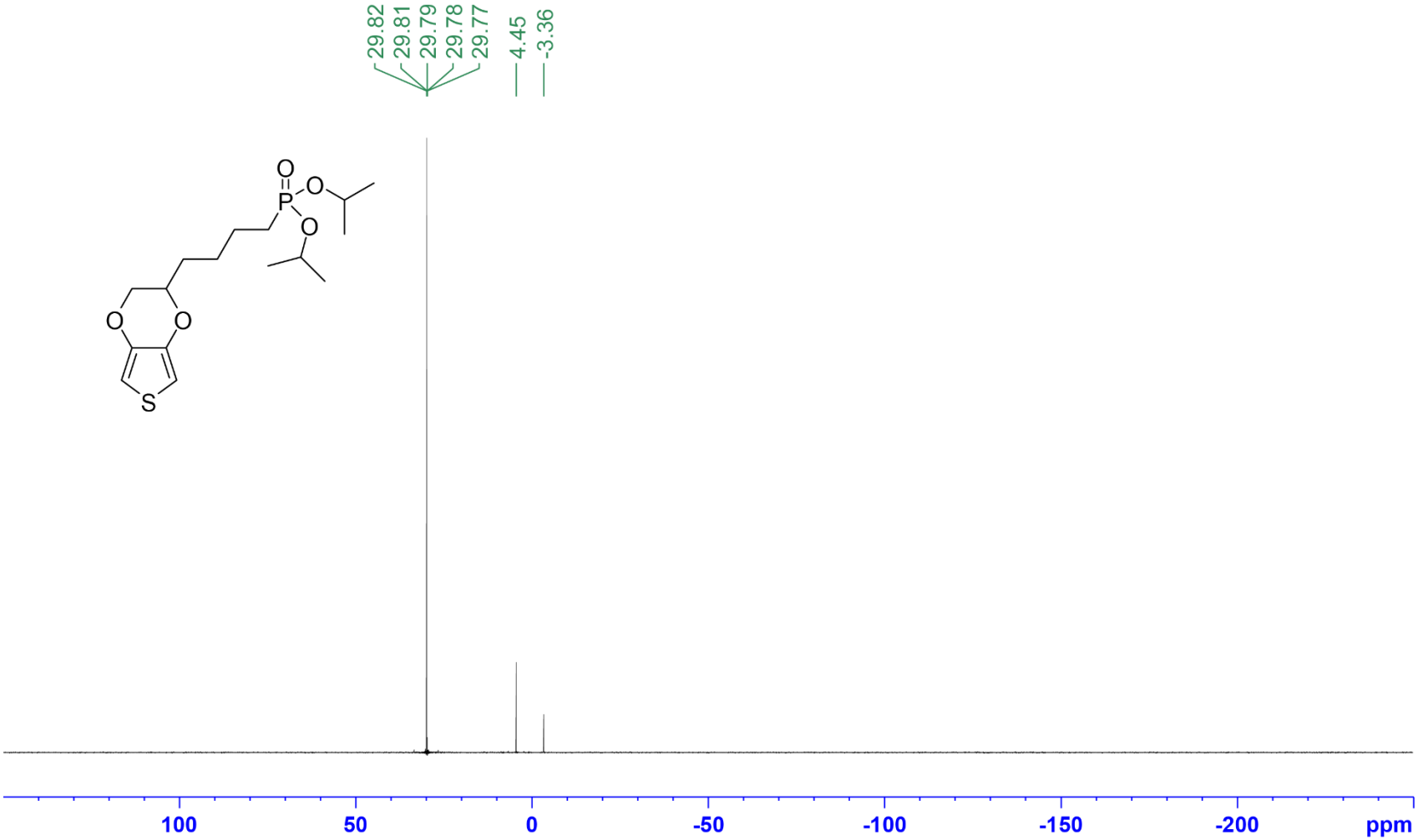

Figure S17. $^{31}P\{^{1}H\}$-decoupled NMR spectrum of EDOT-Bu-Phos in $CDCl_3$.

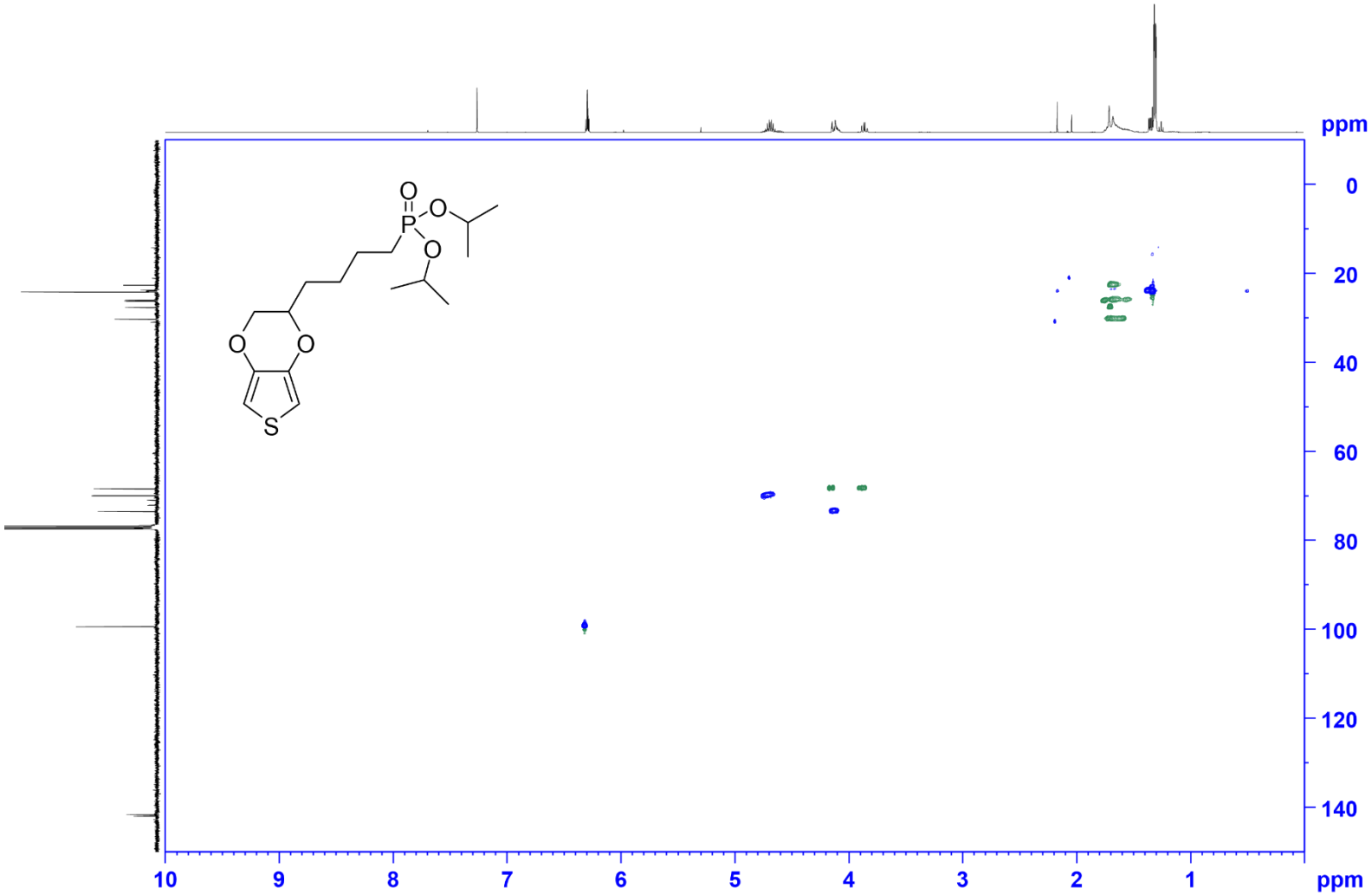

Figure S18. ^{1}H-^{1}3C HSQC NMR spectrum of EDOT-Bu-Phos in $CDCl_3$.

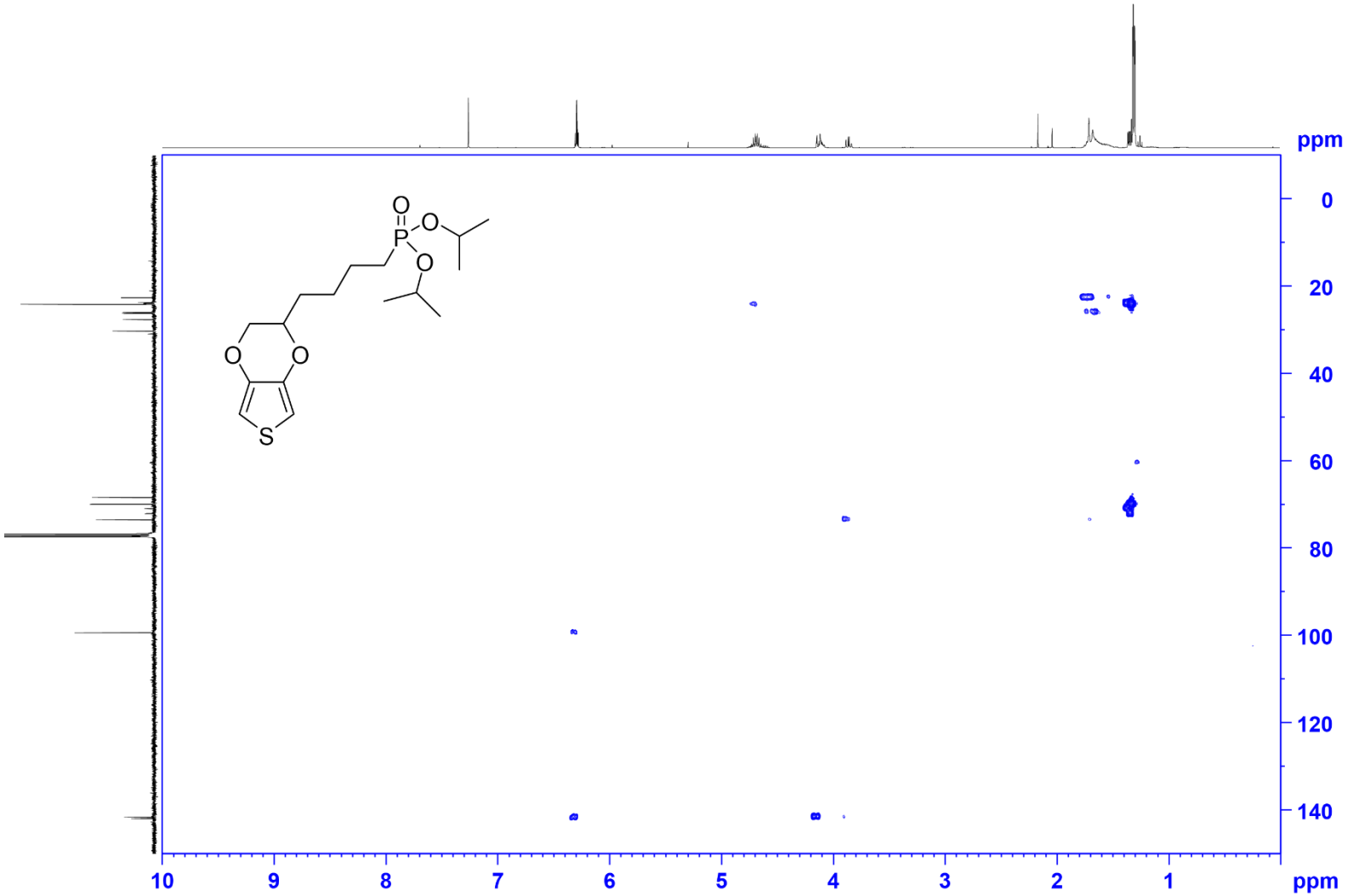

Figure S19. ^{1}H-^{1}3C HMBC NMR spectrum of EDOT-Bu-Phos in $CDCl_3$.

2 FTIR, Raman and XPS characterisation

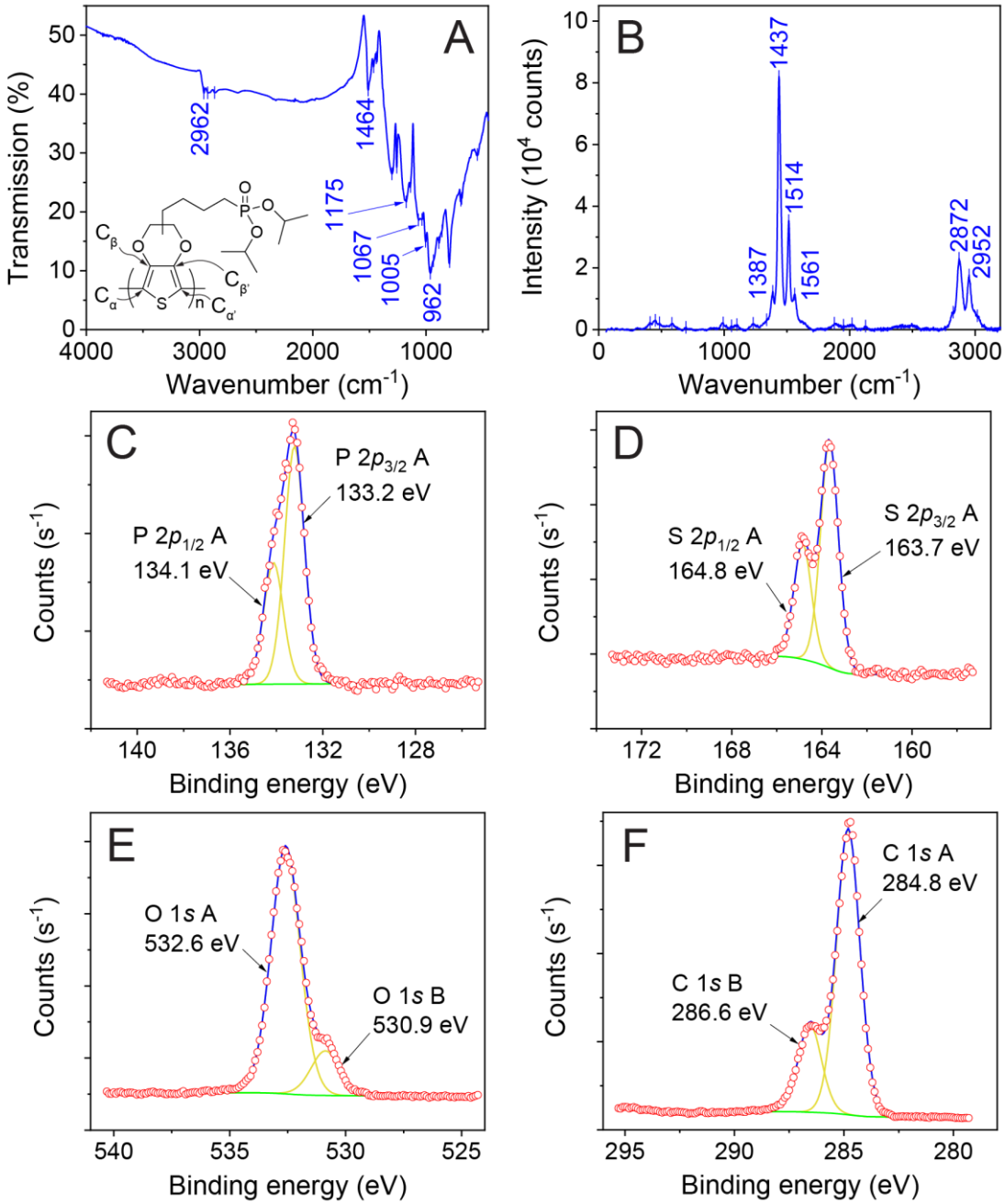

Figure S20. (A) ATR-FTIR spectrum and (B) Raman spectrum (532 nm) of PEDOT-Bu-Phos film on ITO. The chemical structure of PEDOT-Bu-Phos is also shown as an inset of (A) with the α- and β-carbon atoms labelled. (C-F) XPS spectra of PEDOT-Bu-Phos film on ITO showing the (C) P 2*p*, (D) S 2*p*, (E) O 1*s* and (F) C 1*s* environments. The phosphonate P 2*p* signal was seen as a spin-split doublet with the P $2p_{3/2}$ peak at binding energy 133.2 eV and the thiophene sulfur S 2*p* signal appeared as a doublet with the S $2p_{3/2}$ peak at 163.7 eV. The strong O 1*s* signal at 532.6 eV likely corresponds to the ethylenedioxy oxygen atoms, while the smaller signal at 530.9 eV likely includes contributions from the oxygen atoms in the phosphonate

group. The carbon C 1*s* peak at 284.8 eV was assigned to thiophene and aliphatic carbon atoms, and a weaker peak at 286.6 eV resulted from carbon atoms in the C-P bond with the phosphonate group and in C-O bonds in the ethylenedioxy bridge.

Table S1. Assignment of peaks observed in ATR-FTIR and Raman spectroscopy of PEDOT-Bu-Phos. C_α and C_β denote the α- and β-carbon atoms in the structure of PEDOT-Bu-Phos shown in Figure S20A.

Description	**ATR-FTIR (cm^{-1})**	**Raman (cm^{-1})**	**References**
Aliphatic CH_2 stretch	---	3018	[1,2]
Aliphatic CH_2/CH_3 stretch	2962	2952	[1,2]
Aliphatic CH_2/CH_3 stretch	2927	2872	[1,2]
Aliphatic CH_2 stretch	2868	2824	[1,2]
Aliphatic CH_2 bend	---	1561	[2]
Asymmetric C_α=C_β stretch	1512	1514	[1,2]
Aliphatic CH_2 bend	1464	---	[3]
Symmetric C_α=C_β(-O) stretch	1439	1437	[1]
Thiophene C_β–C_β stretch	---	1387	[1,2]
Aliphatic CH_2 twist	1302	1338	[2]
C_α=$C_{\alpha'}$ inter-ring stretch	1259	1264	[1,4]
Phosphonate P=O stretch	1175	---	[5]
C_α=$C_{\alpha'}$ inter-ring stretch	---	1231	[1]
Phosphonate O-P-O stretch + C-O-C deform	1067	1101	[1,5,6]
Phosphonate (P-)O-C stretch	1035	---	[6]
Phosphonate P-O(-C) stretch + C-O stretch	1005	---	[2,5,6]
Ethylenedioxy ring deform	---	992	[2]
Phosphonate (P-)O-C stretch	962	---	[2,5,6]
Phosphonate (C-)P-O stretch	887	---	[5,6]
Ethylenedioxy ring deform	792	---	[1,2]
Ethylenedioxy CH_2 rocking	693	---	[2]
Symmetric C-S-C deform	683	694	[2]
Ethylenedioxy ring deform	---	584	[1,2]
C-O-C deform	---	451	[1,2]

3 Morphological characterisation

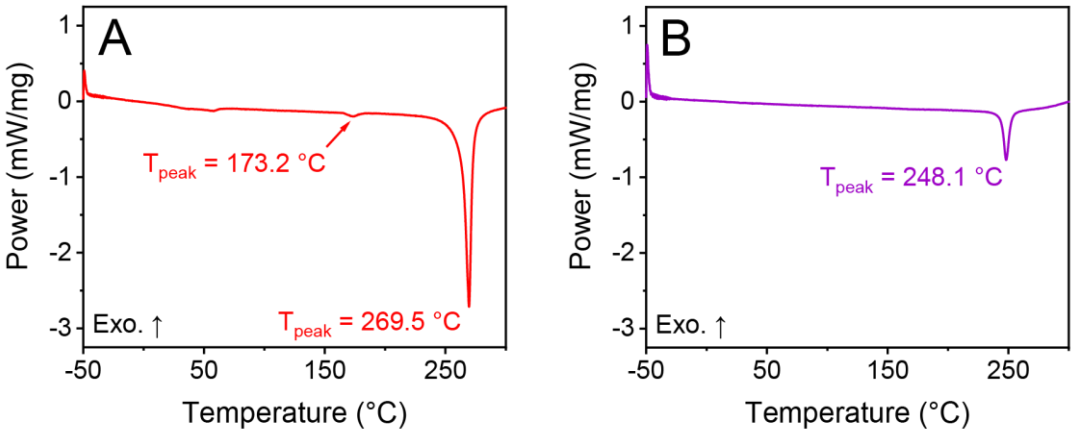

Figure S21. (A-B) DSC heating curves of (A) PEDOT-Bu-Phos and (B) PEDOT-Phos.

Table S2. Summary of peak positions observed in the integrated GIWAXS data for both polymers, before and after CV.

PEDOT-Phos (nm^{-1} / Å)		PEDOT-Bu-Phos (nm^{-1} / Å)	
Before CV	**After CV**	**Before CV**	**After CV**
3.29 / 19.1	3.31 / 19.0	2.73 / 23.0	2.91 / 21.6
--- / ---[a]	--- / ---[a]	5.17 / 12.2	5.13 / 12.2
--- / ---[a]	--- / ---[a]	14.1 / 4.46	14.2 / 4.42
14.7 / 4.27	--- / ---[a]	14.4 / 4.36	14.4 / 4.36
15.2 / 4.13	15.2 / 4.13	15.2 / 4.13	15.2 / 4.13
--- / ---[a]	--- / ---[a]	16.1 / 3.90	16.1 / 3.90
16.9 / 3.72	16.9 / 3.72	16.9 / 3.72	16.9 / 3.72

[a] Peak was not observed.

4 Optical and electrochemical characterisation

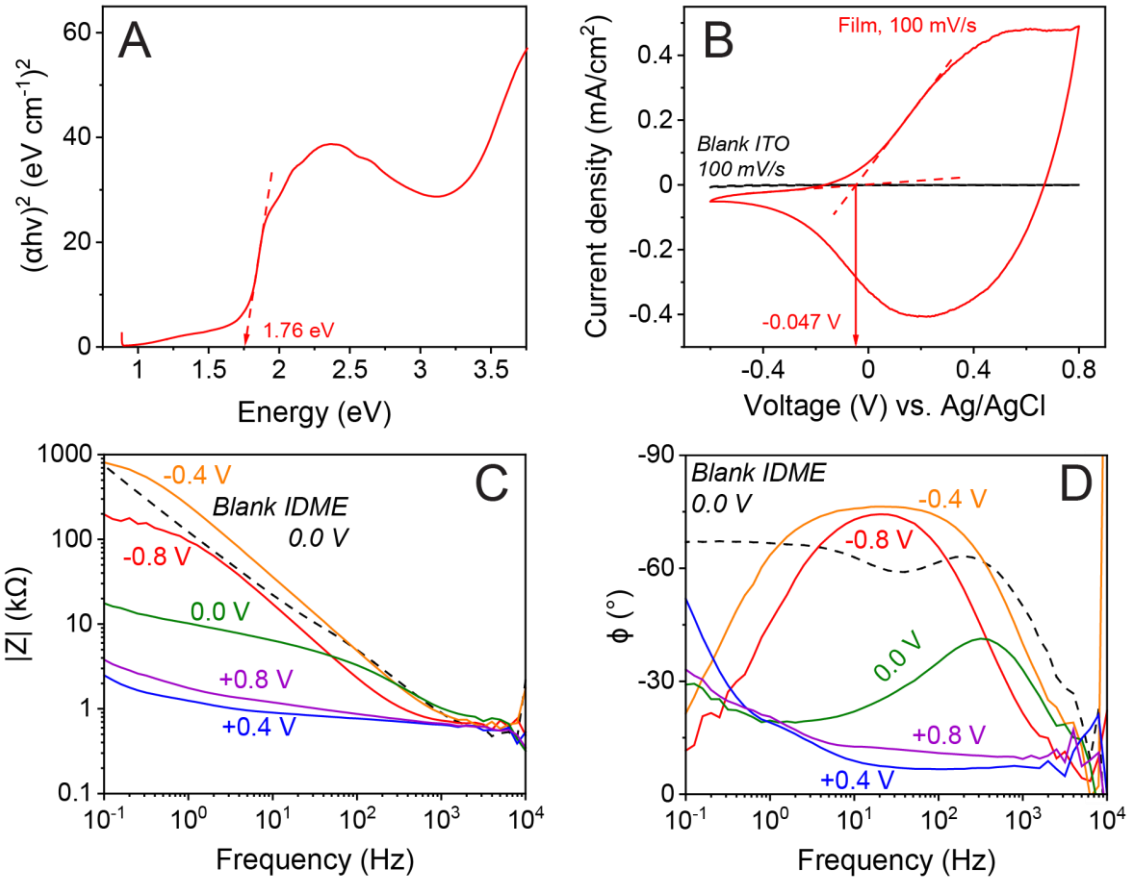

Figure S22. Optical and electrochemical characterisation: (A) Tauc plot of a pristine PEDOT-Bu-Phos film, with the optical band gap energy indicated. (B) Cyclic voltammetry of PEDOT-Bu-Phos on ITO in aqueous NaCl (0.1 M), over the potential range from –0.6 V to +0.8 V. (C-D) EIS of PEDOT-Bu-Phos on an IDME at various applied potentials: (C) Bode impedance and (D) phase plots.

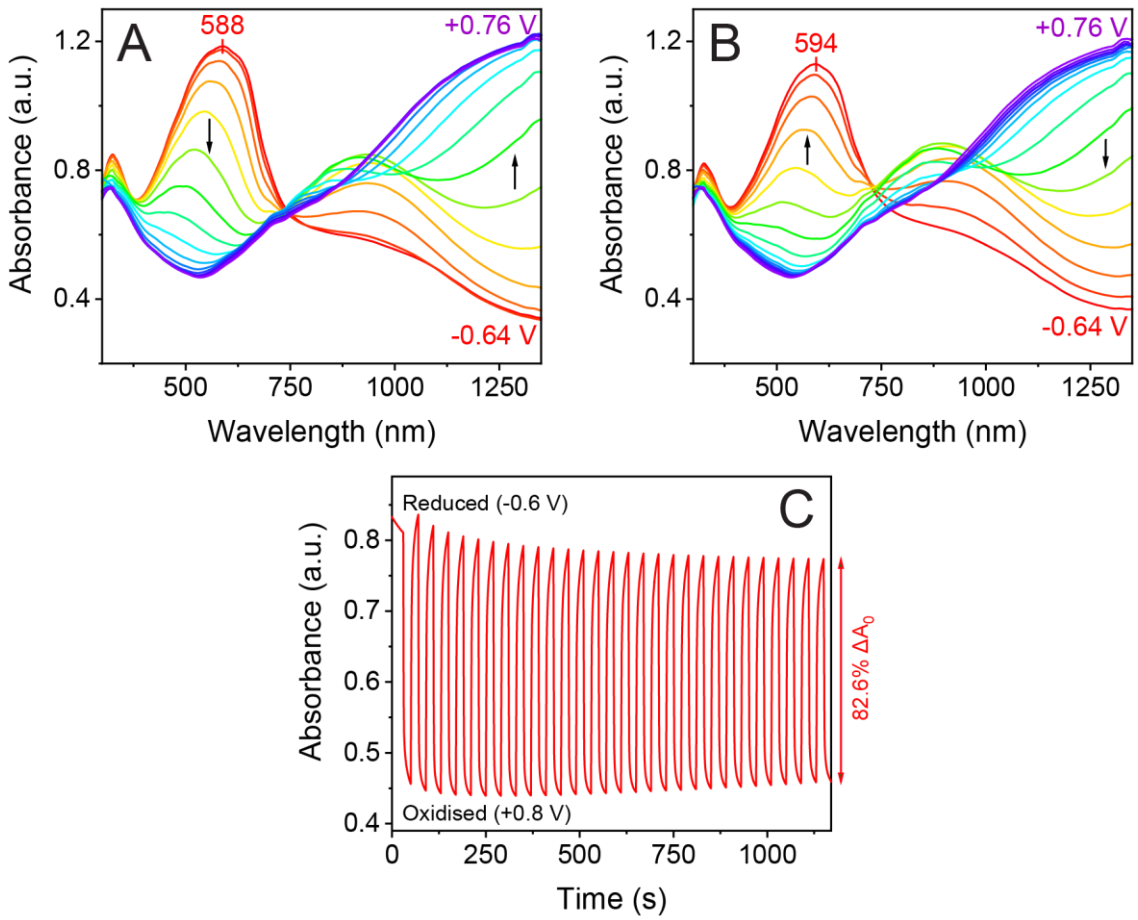

Figure S23. Spectroelectrochemical characterisation: (A-B) *In-situ* UV-vis-NIR spectroelectrochemistry of PEDOT-Bu-Phos on ITO in NaCl (0.1 M in deionised water), with (A) increasing and (B) decreasing potential. The potentials were recorded vs. Ag wire and are reported here relative to Ag/AgCl (= Ag wire – 0.34 V). Counter-electrode: Pt wire. (C) Electrochromic stability: Transient absorbance profile of PEDOT-Bu-Phos on ITO in aqueous NaCl (0.1 M) during *in-situ* double-step spectrochronoamperometry cycling between reduced (–0.6 V) and oxidised (+0.8 V) states.

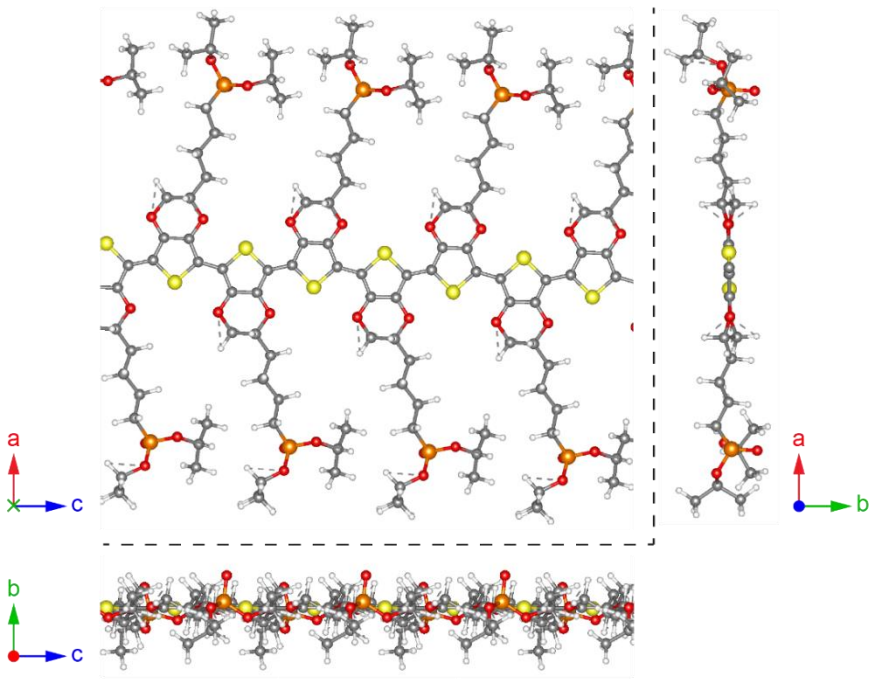

Figure S24. Geometry-optimised molecular models of PEDOT-Bu-Phos as a single molecule. Atoms are C (grey), H (white), O (red), P (orange), S (yellow).

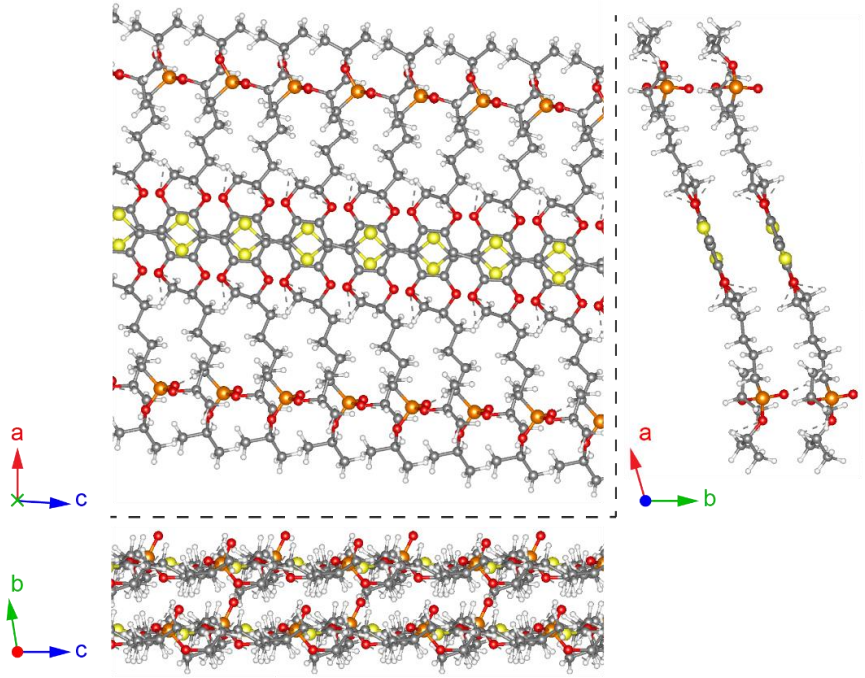

Figure S25. Geometry-optimised molecular models of PEDOT-Bu-Phos as a crystalline solid. Atoms are C (grey), H (white), O (red), P (orange), S (yellow).

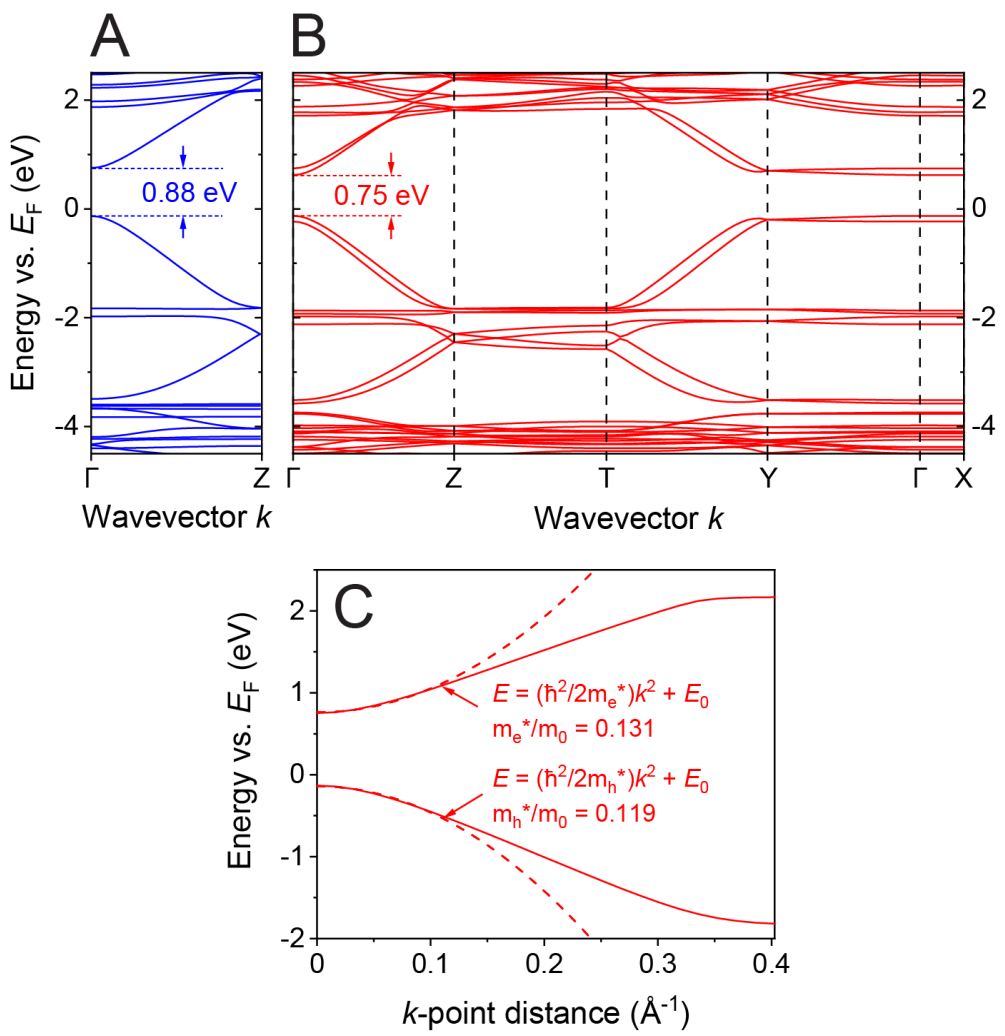

Figure S26. DFT characterisation of PEDOT-Bu-Phos. (A-B) Band structures of (A) an isolated molecule and (B) a crystal, close to the Fermi level (E_F = 0 eV). The indicated high-symmetry points are Γ = (0, 0, 0), Z = (0, 0, 0.5), T = (0, 0.5, 0.5), Y = (0, 0.5, 0), X = (0.5, 0, 0). The theoretical direct bandgap is taken from the band structure as E_g = 0.88 eV. (C) Calculation of effective masses of charge carriers at the conduction and valence band edges in the isolated molecule. The conduction and valence bands were each fitted to a parabola in the region close to zero k-point distance, according to the equation $E = (\hbar^2/2m^*)k^2 + E_0$ where E = energy, E_0 = energy at zero k-point distance, $\hbar$ = Planck's constant, m^* = effective mass of holes (valence band) or electrons (conduction band), and k = the k-point distance. The calculated effective masses are indicated on the figure: m_h^*/m_0 = 0.119, m_e^*/m_0 = 0.131. For PEDOT-Phos[7], the corresponding values are: m_h^*/m_0 = 0.111, m_e^*/m_0 = 0.121.

5 OECT characterisation

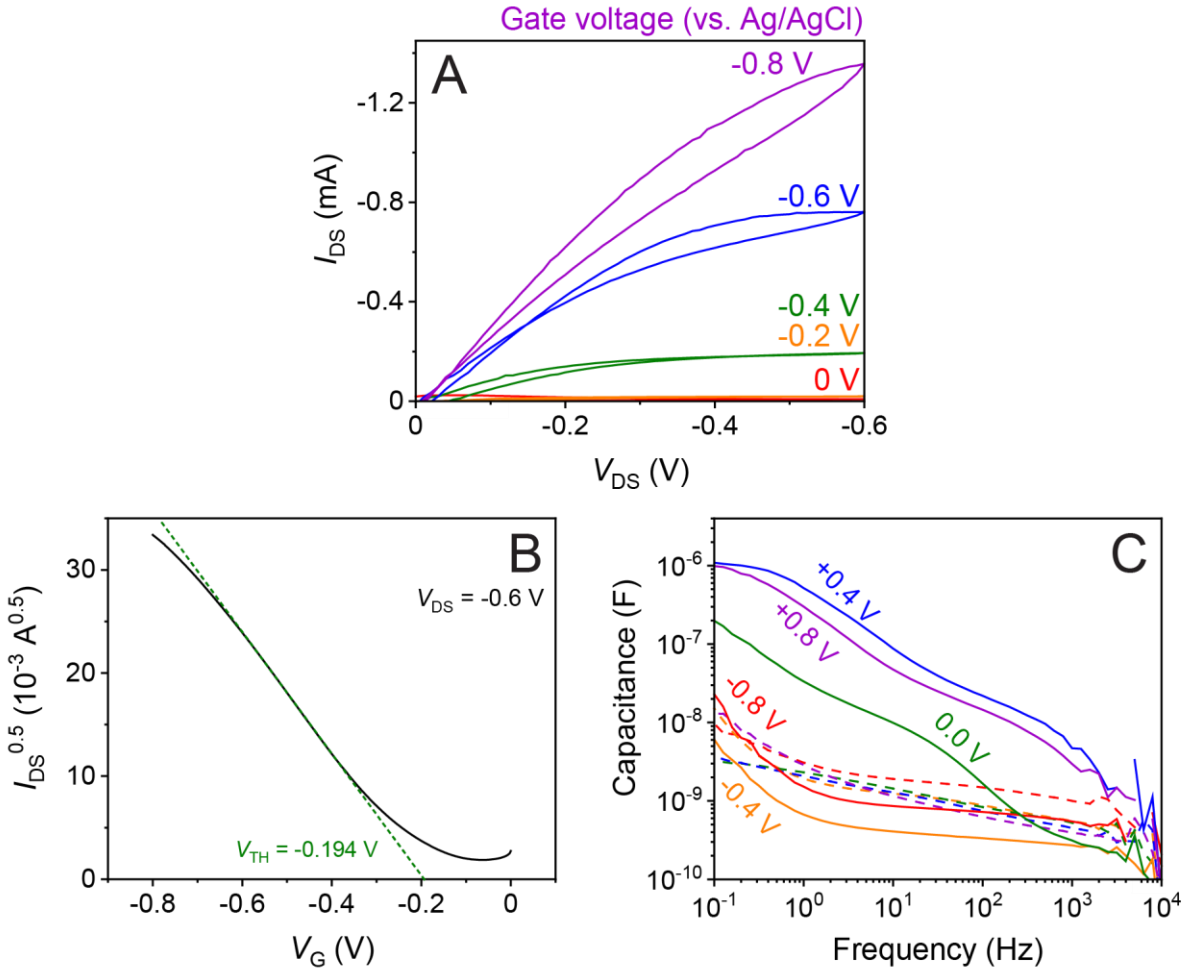

Figure S27. OECT characterisation: (A) Output curves of a representative PEDOT-Bu-Phos OECT in aqueous NaCl at several gate potentials. (B) Calculation of threshold voltage of PEDOT-Bu-Phos in a representative aqueous OECT. (C) Capacitance as a function of frequency of PEDOT-Bu-Phos on an IDME in 0.1 M NaCl at various applied potentials during EIS.

Table S3. Summary of device performance parameters for PEDOT-Bu-Phos OECTs in aqueous NaCl (0.1 M). The channel dimensions are 10 μm (length) × 50 cm (width). ***d* = film thickness;** $g_{m,max}$ = maximum transconductance; **$g_{m,max}/d$ = thickness-normalised maximum transconductance;** $V_{G,max}$ = gate voltage at the maximum transconductance; V_{TH} = threshold voltage; d = film thickness from profilometry; I_{ON}/I_{OFF} = on/off current ratio at V_{DS} = –0.6 V, comparing I_{DS} at –0.8 V (ON) and 0 V (OFF) from the transfer curve; C = capacitance from EIS spectroscopy at +0.4 V; C^* = volumetric capacitance; μ_{OECT} = charge carrier mobility**; μC^* = product of mobility and volumetric capacitance**.

Device	d (nm)	$g_{m,max}$ (mS)	$g_{m,max}/d$ (S cm^{-1})	$V_{G,max}$ (V)	V_{TH} (mV)	I_{ON}/I_{OFF}	C (mF)	C^* (F cm^{-3})	$\mu_{OECT} \times 10^7$ (cm^2 V^{-1} s^{-1})	$\mu C^* \times 10^5$ (F cm^{-1} V^{-1} s^{-1})
1	1457 ± 323	1.7	**11.7**	–0.66	–182	229	0.57	40 ± 9	1.62	0.66
2	1794 ± 214	2.3	**12.6**	–0.78	–178	117	0.81	47 ± 6	3.39	1.60
3	1873 ± 289	2.9	**15.2**	–0.44	–194	148	1.09	61 ± 9	2.47	1.50
Avg. ± Err.[a]	1708 ± 161	2.3 ± 0.6	**13.2 ± 1.8**	–0.63 ± 0.17	–185 ± 8	165 ± 58	0.82 ± 0.26	49 ± 5	2.49 ± 0.88	1.25 ± 0.19

[a] The overall average values of d, C, and C^* are given as average ± error calculated using error propagation. All other values with uncertainties are given as average ± standard deviation.

6 References

[1] S. Garreau, G. Louarn, J. P. Buisson, G. Froyer, S. Lefrant, *Macromolecules* **1999**, *32*, 6807.

[2] F. Tran-Van, S. Garreau, G. Louarn, G. Froyer, C. Chevrot, *J. Mater. Chem.* **2001**, *11*, 1378.

[3] D. K. Kakati, R. Gosain, M. H. George, *Polymer (Guildf).* **1994**, *35*, 398.

[4] Q. Zhao, R. Jamal, L. Zhang, M. Wang, T. Abdiryim, *Nanoscale Res. Lett.* **2014**, *9*, 1.

[5] M. Xu, X. Han, T. Wang, S. Li, D. Hua, *J. Mater. Chem. A* **2018**, *6*, 13894.

[6] I. N. Smirnova, A. Cuisset, F. Hindle, G. Mouret, R. Bocquet, O. Pirali, P. Roy, *J. Phys. Chem. B* **2010**, *114*, 16936.

[7] J. Hopkins, K. Fidanovski, L. Travaglini, D. Ta, J. Hook, P. Wagner, K. Wagner, A. Lauto, C. Cazorla, D. Officer, D. Mawad, *Chem. Mater.* **2022**, *34*, 140.